

## Molecular Dynamics Simulation of Crystal-Induced Membranolysis

Andrzej Wierzbicki,<sup>\*,†</sup> Pranav Dalal,<sup>‡</sup> Jeffrey D. Madura,<sup>‡</sup> and Herman S. Cheung<sup>§</sup>

Department of Chemistry, University of South Alabama, Mobile, Alabama 36688, Department of Chemistry and Biochemistry, Duquesne University, Pittsburgh, Pennsylvania 15282, and Department of Biomedical Engineering, University of Miami, and Geriatric Research, Education, and Clinical Center, V.A. Medical Center, Miami, Florida 33135

Received: May 8, 2003; In Final Form: August 11, 2003

Calcium pyrophosphate dihydrate (CPPD) crystals occur frequently in noninflammatory osteoarthritic joints; however, they can be phlogistic and membranolytic, causing acute pseudogout attack. So far, the molecular mechanism of crystal-induced membranolysis is still unclear. In this study, using the method of Chemistry at Harvard Macromolecular Mechanics (CHARMM) molecular dynamics, we show that the interactions between the surface of CPPD crystal and the extracellular layer of the hydrated dimyristoyl phosphatidylcholine (DMPC) phospholipid bilayer may lead to decoupling of the external layer from the intracellular side of the membrane. As a result, a local thinning of the layer on the intracellular side of the membrane occurs, which favors water penetration, leading to membranolysis.

### Introduction

Crystalline calcium pyrophosphate dihydrate (CPPD) crystals are among the most common forms of pathologic articular mineral. CPPD crystal deposition increases in prevalence with aging; its prevalence increases to 50% at the age of 90 years.<sup>1</sup> Although they occur frequently in noninflammatory osteoarthritic (OA) joints, they can be phlogistic, causing acute attacks of pseudogout.<sup>2,3</sup>

Crystal surface charge and morphology are important determinants of the inflammatory potential of crystals. The surface of the more-inflammatory membranolytic crystals, such as monosodium urate, CPPD, and the  $\alpha$ -quartz form of silicon dioxide are irregular and possess a high density of negatively charged groups, in comparison to nonmembranolytic smooth surface crystals, e.g., diamond dust and the anatase form of silicon dioxide. Lesser negatively surface-charged brushite and hydroxyapatite crystals are not often associated with acute inflammation.<sup>4</sup>

A proposed mechanism of inflammation in crystal-induced diseases is dependent on the rupture of the lysosome phospholipid membrane and the release of lysosomal enzymes into the cytoplasm.<sup>5</sup> So far, there is no direct evidence that the crystal–membrane interaction may lead to membrane immobilization and possibly rupture, although some indirect evidence of the crystal–cell interactions has been already presented. For example, it has been demonstrated that the adhesion of calcium oxalate monohydrate (COM) crystals involves anionic sites on the surface of renal epithelial cells.<sup>6,7</sup> In another related study involving different classes of anionic crystals, namely hydroxyapatite, it has been also speculated that the interaction between renal epithelial cells and hydroxyapatite crystal surfaces involves negatively charged molecules protruding from the apical surface of the plasma membrane.<sup>8</sup>

Numerous experimental investigations have revealed great complexity of the membrane dynamics, both alone and in the presence of embedded transmembrane proteins.<sup>9–16</sup> Despite a wealth of experimental data, however, no microscopic insight into the nature of crystal-induced membranolysis can be gained without a detailed molecular model of the membrane–crystal interactions. To our knowledge, no such model has been proposed so far. Understanding of these interactions at the molecular level would be extremely helpful, not only to elucidate the molecular nature of cell–crystal interaction but also to aid in the design of therapeutic agents that could diminish such an interaction. There is already some experimental evidence that phosphocitrate, which is a polyanion, protects from crystal-induced polymorphonuclear leukocyte membranolysis.<sup>17</sup>

Interestingly, quite advanced theoretical investigations of the rupture of phospholipid bilayers have been undertaken for systems involving lysis of the phospholipid membranes not by inorganic crystal surfaces but by small proteins. For some time now, there has been an intensive effort undertaken to elucidate the membranolysis induced by melittin, which is a small  $\alpha$ -helical protein from honey bee venom that is known to rupture cell membranes.<sup>18–20</sup> The 26-amino-acid-long peptide is the principal toxic component of the venom of the honey bee,<sup>20,21</sup> which spontaneously binds to lipid bilayers and acts as a lytic agent.<sup>20</sup> Extensive molecular dynamics (MD) studies have revealed that the binding of melittin to the extracellular layer of the membrane causes the perturbation of both extra and intracellular layers of the phospholipid membrane,<sup>18–20</sup> with surprisingly much greater impact on the intracellular layer. The lytic mechanism induced by the binding of melittin to the extracellular layer is dramatically accentuated by water penetration proceeding mainly from the intracellular side of the bilayer.

In this study, we investigate the CPPD crystal-induced membranolysis of the dimyristoyl phosphatidylcholine (DMPC) phospholipid bilayer. The DMPC phospholipid (Figure 1) constitutes a building element of this bilayer, and it is the most prevalent phospholipid among those that comprise eukaryotic cell membranes.<sup>22</sup> We show that the progress of crystal-induced membranolysis is very similar to the lysis induced by melittin.

\* Author to whom correspondence should be addressed. E-mail: awierzbi@jaguar1.usouthal.edu.

<sup>†</sup> University of South Alabama.

<sup>‡</sup> Duquesne University.

<sup>§</sup> University of Miami and Geriatric Research, Education, and Clinical Center, V.A. Medical Center.

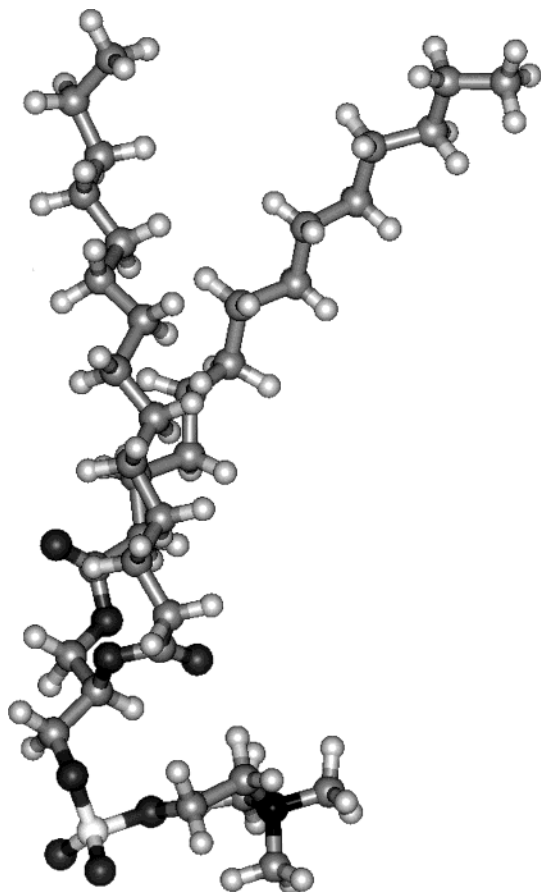


**Figure 1.** Conformation of the DMPC molecule used to build the phospholipid bilayer discussed in this study. Unique conformations are randomly selected from a pre-equilibrated and pre-hydrated set generated from Monte Carlo simulations of an isolated DMPC molecule.

## Methods

The solvated DMPC lipid bilayer was generated using the “membrane module” available in the support directory of Chemistry of Harvard Macromolecular Mechanics (CHARMM) software.<sup>23</sup> The protocol in this module was developed with the purpose of constructing an initial configuration of a protein–membrane complex that is as similar as possible to that of an equilibrated system. The construction method was developed by Woolf and Roux and applied to the simulation of gramicidin and pf1.<sup>24,25</sup> In brief, the general strategy for creating a reasonable starting configuration for a phospholipid system consisted of randomly selecting lipids from a pre-equilibrated and pre-hydrated set and then placing them in a bilayer. The number of core–core overlaps between heavy atoms were reduced through systematic rotations (around the *z*-axis) and translations (in the *xy* plane) of the lipids. The system was then equilibrated by performing MD simulation. Equilibrated water boxes were subsequently placed near the headgroups of the lipid molecules, resulting in a total of 13 860 atoms. The resulting system size was 88 Å tall, from the edge of one water box across the bilayer to the edge of the opposite water box, and the cross-sectional dimensions were 48 Å × 32 Å. After the solvated lipid bilayer was generated, it was equilibrated for 200 ps, during which time the potential energy of the system converged. Equilibration was quickly achieved, because the lipid molecules were obtained from a pre-equilibrated and pre-hydrated set. Subsequently, the water molecules were removed and the CPPD (010) crystal was placed near one of the leaflets of the lipid bilayer. A Monte Carlo simulation was performed at this point

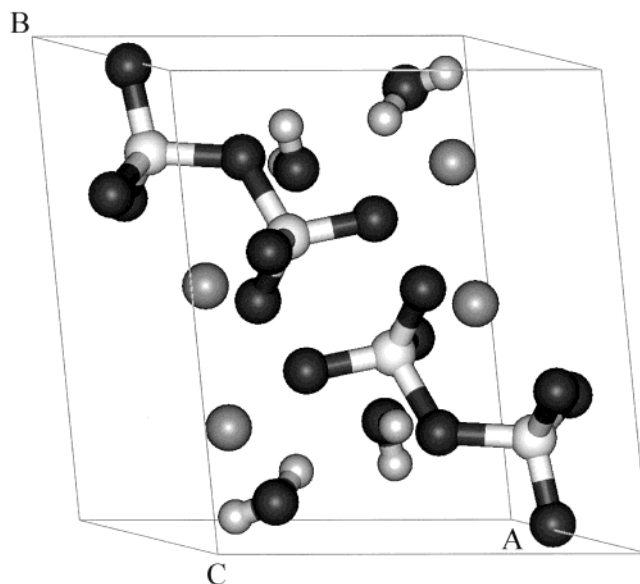


**Figure 2.** Unit cell of CPPD crystal derived from the X-ray data of the triclinic structure of CPPD crystal given in ref 30.

(5000 steps) to identify the most favorable position by determining the most favorable interaction energy of the CPPD crystal on the lipid bilayer. Upon identifying the position of the CPPD crystal on the lipid bilayer, the water was reintroduced in the system. The water molecules within 2.5 Å of the crystal were then removed, resulting in a system size of 13 579 atoms. During these simulations, the CPPD crystal was held fixed. The entire system was then subjected to 10 000 steps of steepest-descent minimization. A thermalization step of 30 ps was subsequently performed to bring the system to 300 K. Finally, constant-pressure and temperature (CPT) dynamics (1 bar, 300 K) were performed, using a Nose–Hoover thermostat and barostat. The simulation was conducted for 600 ps, using a time step of 2 fs. Ewald summations were used for long-range electrostatics. During the CPT simulation, the SHAKE algorithm was used to constrain all bonds involving H atoms. An identical control simulation was conducted for the lipid bilayer without the CPPD crystal.

The TIP3P parameters<sup>26</sup> were used for the water molecules, and all-atom CHARMM parameters<sup>27</sup> were used for the lipid bilayer. In the CHARMM force field, the DMPC molecules are parametrized, such that an individual molecule has no net charge.<sup>28</sup> Nonbonded interactions were cut off at 14 Å. Hence, there was no need to add any counterions for the MD simulation. Standard CHARMM parameters were modified to obtain the CPPD crystal parameters.

The (010) slabs of triclinic CPPD (Figure 2) were created, following the procedure described earlier<sup>29</sup> from the data provided by X-ray crystallography.<sup>30</sup> Using Cerius<sup>2</sup> software,<sup>31</sup> we prepared a neutral slab of CPPD crystal, parallel to the (010) crystallographical planes. The resulting 4 × 4 × 1 crystal was composed of 544 atoms and had dimensions of 34.7 Å × 30.2 Å × 8.7 Å. Molecular and atomic charges of the surfaces were determined using the charge equilibration method.<sup>32</sup>

## Results

Figures 3 and 4 are plots in which we have calculated the average position of the atoms across the solvated lipid bilayer over 200 ps. The positions are shown averaged over 0–200, 200–400, and 400–600 ps. The plots show the number of water O atoms (Figure 3a) and the headgroup N atoms of the lipid

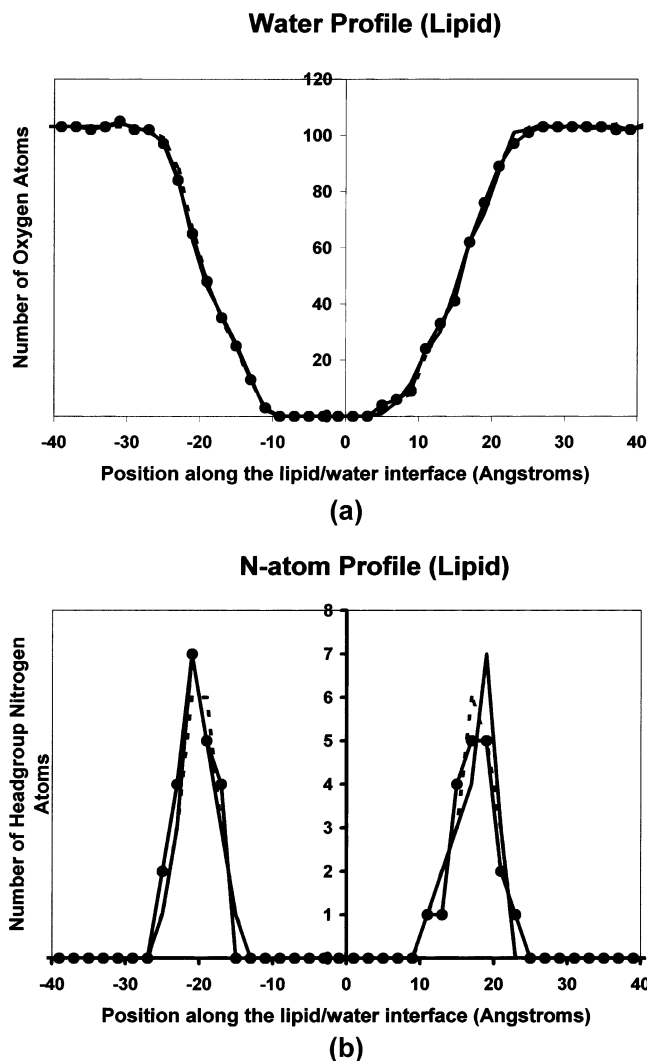


**Figure 3.** (a) Number of O atoms of the water molecules and (b) number of lipid headgroup N atoms along the water/lipid interface when no CPPD crystal is present. Data are presented as time-averaged series. Averages in the ranges of (—) 0–200, (—●—) 200–400, and (---) 400–600 ps are presented. The position along the lipid/water interface is denoted on the *x*-axis, with 0 being the center of the bilayer, whereas the number of atoms is plotted on the *y*-axis. Negative coordinates are located below the center of the bilayer, and positive coordinates are located above the center (see Figures 5 and 6).

molecules (Figure 3b) across the water/lipid interface in the solvated lipid bilayer without the crystal. For the solvated bilayer (without the crystal) (Figure 3a), we observe that the water molecules are outside the bilayer and they do not penetrate into the bilayer throughout the simulation. The headgroup N atoms are distributed evenly, and majority of them lie in the same plane (see Figure 3b). These properties are also evident in Figure 5. This figure represents snapshots obtained at intervals of 200 ps during the simulation. It is clearly evident that the integrity of the lipid bilayer is maintained. Figure 4a and b depict the same properties as in Figure 3a and b, albeit with a CPPD crystal placed at one of the water/lipid interfaces. In Figure 4a, it is evident that water molecules penetrate the lipid bilayer. The dip observed in Figure 4a on the left-hand side is due to the crystal replacing some of the water molecules in that region. Furthermore, the N atoms (Figure 4b) are also not uniformly positioned, in comparison to those in Figure 3b. An interesting observation is that the N atoms are more disproportionate in the layer away from the crystal. This is also observed in snapshots shown in Figure 6. The lipid layer near the crystal is

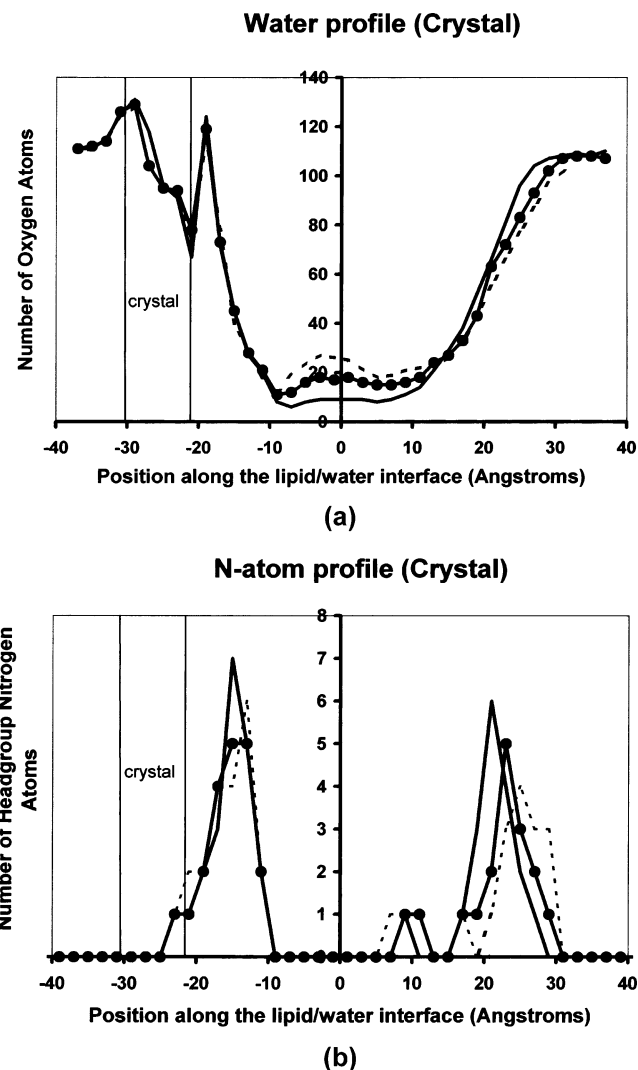


**Figure 4.** (a) Number of O atoms of the water molecules and (b) number of lipid headgroup N atoms along the water/lipid interface when the CPPD crystal is present at one of the lipid/water interfaces. Data are presented as time-averaged series. Averages in the ranges of (—) 0–200, (—●—) 200–400, and (---) 400–600 ps are presented. The position along the lipid/water interface is denoted on the *x*-axis, with 0 being the center of the bilayer, whereas the number of atoms is plotted on the *y*-axis. Negative coordinates are located below the center of the bilayer, and positive coordinates are located above the center (see Figures 5 and 6). The position of the crystal is marked on the left portion of the plot with two lines.

maintained more uniformly. To test this hypothesis further, we placed the crystal on the opposite side and repeated the calculations. We noticed that the lipid layer near the crystal was more uniform and the lipid layer away from the crystal was nonuniform, leading to a loss of the integrity of the lipid bilayer, followed by penetration by the water molecules.

To test the hypothesis that the interaction with the crystal stabilizes and reduces the mobility of the lipids, we calculated the diffusion coefficient of the N atoms of the lipid headgroup. In the simulation involving only the lipid bilayer, the diffusion coefficient of the N atoms of the lipid headgroup was relatively similar. For the bottom layer, we calculated a value of  $0.55 \times 10^{-2} \text{ \AA}^2/\text{ps}$  ( $\pm 0.9 \times 10^{-4} \text{ \AA}^2/\text{ps}$ ); for the top layer, we calculated a value of  $0.69 \times 10^{-2} \text{ \AA}^2/\text{ps}$  ( $\pm 0.16 \times 10^{-3} \text{ \AA}^2/\text{ps}$ ). However, the values were quite different for the simulations in which we placed the crystal at the bottom lipid leaflet. In those simulations, for the bottom layer (interacting with crystal), we obtained a value of  $0.16 \times 10^{-2} \text{ \AA}^2/\text{ps}$  ( $\pm 0.1 \times 10^{-4} \text{ \AA}^2/\text{ps}$ ), whereas for

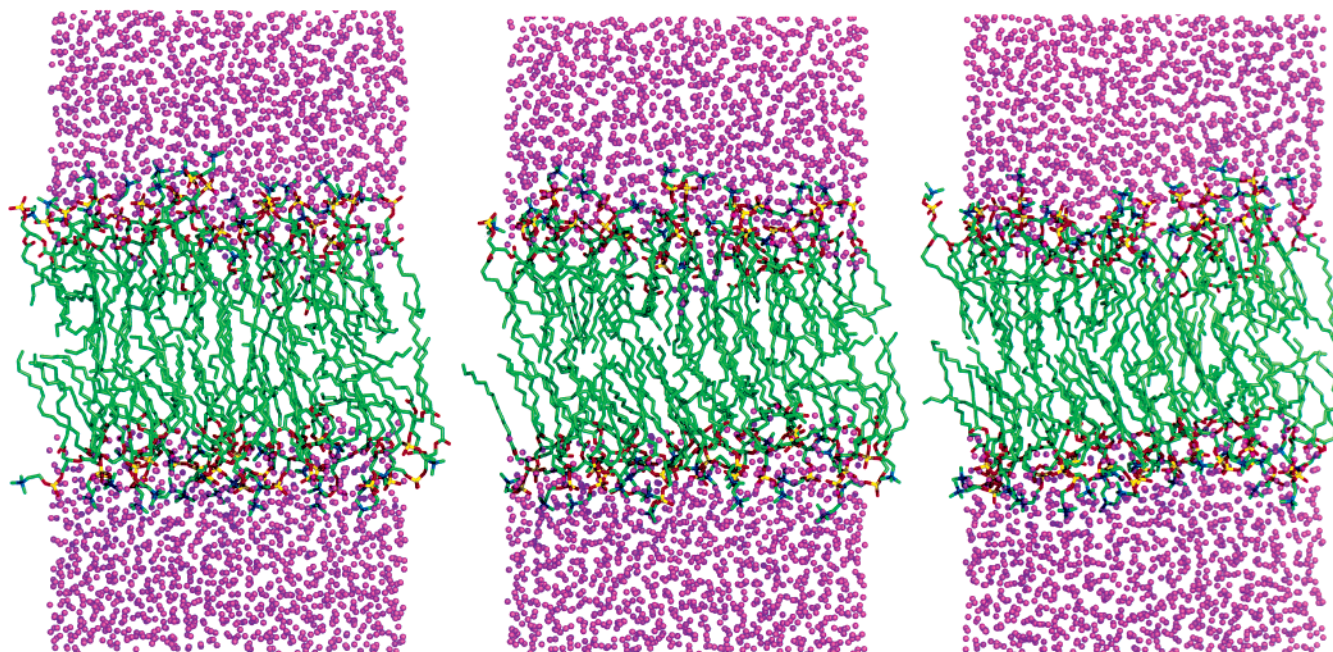


**Figure 5.** Snapshots from the simulation of a solvated lipid bilayer at different time points. Magenta spheres indicate the O atoms of the water molecules, and the lipid molecules are shown as chains; the C atoms are shown in green, P atoms in yellow, O atoms in red, and N atoms in blue. Each snapshot is 200 ps apart, time advancing from left to right.

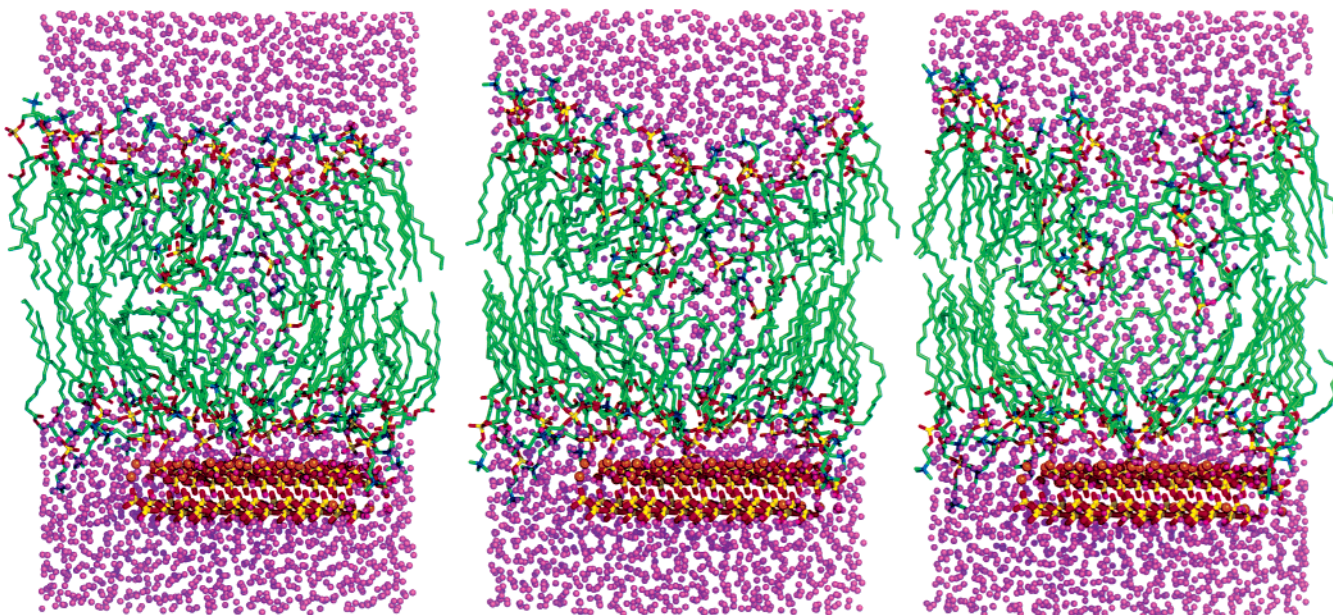


**Figure 6.** Snapshots from the simulation of a solvated lipid bilayer with a CPPD crystal at the lipid/water interface. Magenta spheres indicate the O atoms of the water molecules, and the lipid molecules are shown as chains. Hydrocarbon chains are shown in green. Crystal is depicted at the lower lipid/water interface, using the ball-and-stick scheme. Snapshots shown here are 200 ps apart, time advancing from left to right.

the top layer, we obtained a value of  $0.24 \times 10^{-1} \text{ \AA}^2/\text{ps}$  ( $\pm 0.21 \times 10^{-3} \text{ \AA}^2/\text{ps}$ ). Thus, we observe that the diffusion of lipid headgroups is lower (compared to control) in the leaflet interacting with the crystal but larger in the opposite layer.

## Discussion

In the past decade, there has been substantial progress achieved in the molecular modeling and dynamics of phospholipid bilayer systems. Properties of large, solvated phospholipid bilayer systems have been successfully simulated, and reasonably good agreement has been achieved for the molecular properties of these systems, when compared to available experimental data.<sup>22,33–36</sup> Simulation of the diffusion of small

organic molecules<sup>37</sup> and transmembrane proteins<sup>38–41</sup> and the adhesion forces of lipids in a phospholipid membrane<sup>42</sup> have been successfully described using MD simulations. MD has been also successfully applied to study the binding of melittin, which is one of the components of bee venom, to phospholipid bilayers.<sup>18–20</sup> Bee and snake venoms are known to be hemolytic. One explanation is that both venoms contain a high-level phospholipase (A2), which can cleave the fatty acid residue at C2, leaving a lysophospholipid. Lysophospholipid is a powerful detergent and can disrupt the cell membrane, leading to cell lysis.<sup>43</sup> However, a recent insightful protein-induced membrane disorder study suggested that melittin, one of the components of bee venom, may also be a key player in the mem-

branolysis.<sup>18–20</sup> A significant amount of research effort that was recently put into the field by the MD studies of phospholipid bilayers has made this method a very important tool in gaining insight into the nature of complicated molecular processes that involve phospholipid bilayers. It must be stressed that this progress was possible only through careful calibration of computational methods against a wealth of experimental data that was already available.<sup>44</sup>

In this study, using MD simulations, we were able to follow, for the first time, the molecular mechanism of crystal-induced membranous analysis. We have already shown that, although the surface is neutral overall, it contains the loci of both positive and negative charges, and it is able to attract complementarily charged molecular species, such as the highly negatively charged (–4) phosphocitrate anion.<sup>29</sup> Our earlier investigations (unpublished) involving a continuous dielectric model with the dielectric constant of 80 show that, for both a single DMPC molecule and the phospholipid bilayer used in this study, there exists an attractive electrostatic interaction energy to the neutral (010) slab of CPPD. Accordingly, we propose that the introduction of the neutral (010) slab of CPPD crystals into the close proximity of a hydrated bilayer of DMPC results in the electrostatic attraction between the charged phospholipid headgroups (Figure 6) to the patches of the complementary local charge within the (010) surface of CPPD. The details of this effect are currently under investigation and will be reported later. These headgroups move forward (Figure 6, center panel, and Figure 4b), and the interaction with the crystal stabilizes and decreases the mobility of the external layer of the bilayer. Such immobilization, which directly impacts phospholipid fluidity, has been observed in these simulations, as evidenced from the lower diffusion of the lipid headgroups in contact with the crystal. Furthermore, similar immobilization has been experimentally demonstrated for calcium oxalate crystals binding to inner medullary collecting duct (IMCD) membranes.<sup>45</sup> One can also see that the lipid perturbation on the crystal side is relatively modest. In contrast, at the same time, the internal portion of the bilayer becomes decoupled from the external portion and starts a local thinning right in the middle of the layer (Figure 6, center panel, and Figure 4a). The headgroups mobility calculations indicate that both layers of the free (no crystal) and solvated bilayer have almost-identical mobility. In contrast, the introduction of the (010) crystal surface leads to decreased mobility of the layer adjacent to the crystal and increased mobility of the opposite layer. In this sense, the concerted motion of the layers becomes decoupled. This results in degeneration of the internal bilayer and allows water to penetrate through the internal portion of the bilayer (Figure 6, right panel, and Figure 4a). This previously described remarkable progression of events closely resembles the effect of melittin on the phospholipid bilayer, which has been beautifully demonstrated in independent studies.<sup>18–20</sup> Generally, all these studies show that the insertion of melittin into the external layer of the phospholipid bilayer results in much smaller perturbation of this layer than the adjacent internal layer, which becomes decoupled from the external layer. A preferential increase in the fractional free volume is observed, which, in turn, favors water penetration from the internal side of the bilayer.<sup>20</sup>

Interestingly, another set of simulations (data not shown) that involve palmitoylcholine (POPC) lipid molecules do not show a similar effect. The difference between the effects of CPPD crystal on bilayers consisting of POPC and DMPC lipid molecules is under further investigation.

Studies of the interaction between ionic crystals and phospholipid bilayers<sup>6,17</sup> show that these interactions can be modified

by polyanions such as phosphocitrate,<sup>6,17</sup> citrate, polyaspartate, and polyglutamate.<sup>6</sup> Our earlier molecular modeling studies<sup>29</sup> show that phosphocitrate could be used as a powerful inhibitor of the (010) crystal surfaces of CPPD, which have been shown in this study to be responsible for the interactions with the phospholipid bilayer, which leads to crystal-induced membranous analysis. We believe that by subjecting the CPPD crystals in vivo to phosphocitrate, we could significantly diminish the interactions between the CPPD crystals and phospholipid bilayers, and thus phosphocitrate could serve as a potentially powerful therapeutic agent in crystal-induced arthritic diseases.

**Acknowledgment.** We acknowledge the Pittsburgh Supercomputing Center (through Grant Nos. MCA02N008P and MCB020003P) for their generous allowance of the supercomputer time. Also, we acknowledge the National Institutes of Health (NIH) (through Grant No. AR38421-14) and VA Merit Review for supporting this research.

## References and Notes

- (1) Doyle, D. V. *J. Pathol.* **1982**, *136*, 199.
- (2) Ryan, L. M.; McCarty, D. J. Calcium Phosphate Crystal Deposition Disease, Pseudogout, and Articular Chondrocalcinosis. In *Arthritis and Allied Conditions*, 13th ed.; Koopman, W. J., Ed.; Williams and Wilkins: Baltimore, 1997; p 2103.
- (3) Ryan, L. M.; Cheung, H. S. *Rheum. Dis. Clin. North Am.* **1999**, *25*, 257.
- (4) Terkeltaub, R. A. Pathogenesis and Treatment of Crystal-Induced Inflammation. In *Arthritis and Allied Conditions*, 13th ed.; Koopman, W. J., Ed.; Williams and Wilkins: Baltimore, 1997; Vol. 2, p 2085.
- (5) Mandel, N. S. *Arthritis Rheum.* **1976**, *19*, 439.
- (6) Lieske, J. C.; Norris, R.; Toback, F. G. *Am. J. Physiol.* **1997**, *273*, F224.
- (7) Lieske, J. L.; Toback, F. G.; Deganello, S. *Calcif. Tissue Int.* **1996**, *58*, 195.
- (8) Lieske, J. C.; Leonard, R.; Swift, H.; Toback, F. G. *Am. J. Physiol.* **1996**, *270*, F192.
- (9) Brown, M. F.; Chan, S. I., Eds.; *Bilayer Membranes: Deuterium and Carbon-13 NMR*; Wiley: New York, 1996; p 871.
- (10) Brown, M. F., Ed.; *Membrane Structure and Dynamics Investigated with NMR Spectroscopy*; Birkhäuser: Boston, 1996; p 175.
- (11) Salamon, Z.; Wang, Y.; Soulages, J. L.; Brown, M. F.; Tollin, G. *Biophys. J.* **1996**, *71*, 283.
- (12) Nevzorov, A. A.; Trouard, T. P.; Brown, M. F. *Phys. Rev. E* **1998**, *58*, 2259.
- (13) Trouard, T. P.; Nevzorov, A. A.; Alam, T. M.; Job, C.; Zajicek, J.; Brown, M. F. *J. Chem. Phys.* **1999**, *110*, 8802.
- (14) Salamon, Z.; Brown, M. F.; Tollin, G. *Trends Biochem. Sci.* **1999**, *24*, 213.
- (15) White, S. H.; Wiener, M. C. Determination of the Structure of Fluid Lipid Bilayer Membranes; In *Permeability and Stability of Lipid Bilayers*; Disalvo, E. A., Simon, S. A., Eds.; CRC Press: Boca Raton, FL, 1995; p 1.
- (16) White, S. H.; Wiener, M. C. The Liquid-Crystallographic Structure of Fluid Lipid Bilayer Membranes. In *Biological Membranes*; Merz, K., Jr., Roux, B., Eds.; Birkhäuser: Boston, 1996; pp 127–144.
- (17) Sallis, J. D.; Shankar, R.; Rees, B.; Thomson, R. *Biochem. Med. Metabolic Biol.* **1989**, *41*, 56.
- (18) Berneche, S.; Nina, M.; Roux, B. *Biophys. J.* **1998**, *75*, 1603.
- (19) Lin, J.-H.; Baumgaertner, A. *Biophys. J.* **2000**, *78*, 1714.
- (20) Bachar, M.; Becker, O. M. *Biophys. J.* **2000**, *78*, 1359.
- (21) Terwilliger, T. C.; Weissman, L.; Eisenberg, D. *Biophys. J.* **1982**, *37*, 353.
- (22) Pasenkiewicz-Gierula, M.; Takaoka, Y.; Miyagawa, H.; Kitamura, K.; Kusumi, A. *Biophys. J.* **1999**, *76*, 1228.
- (23) Brooks, B. R.; Brucoleri, R. E.; Olafson, B. D.; States, D. J.; Swaminathan, S.; Karplus, M. *J. Comput. Chem.* **1983**, *4*, 187.
- (24) Woolf, T. B.; Roux, B. *Proc. Natl. Acad. Sci. U.S.A.* **1994**, *91*, 11631.
- (25) Woolf, T. B.; Roux, B. Molecular Dynamics of Pfl Coat Protein in a Phospholipid Bilayer. In *Biological Membranes: A Molecular Perspective from Computation and Experiment*; Merz, K. M., Roux, B., Eds.; Birkhäuser: Boston, 1996; p 555.
- (26) Jorgensen, W. L.; Chandrasekhar, J.; Madura, J. D.; Impey, R. W.; Klein, M. L. *J. Chem. Phys.* **1983**, *79*, 926.
- (27) MacKerell, A. D., Jr.; Bashford, D.; Bellott, M.; Dunbrack, R. L., Jr.; Evanseck, J. D.; Field, M. J.; Fischer, S.; Gao, J.; Guo, H.; Ha, S.;

Joseph-McCarthy, D.; Kuchnir, L.; Kuczera, K.; Lau, F. T. K.; Mattos, C.; Michnick, S.; Ngo, T.; Nguyen, D. T.; Prodhom, B.; Reiher, W. E., III; Roux, B.; Schlenkrich, M.; Smith, J. C.; Stote, R.; Straub, J.; Watanabe, M.; Wiórkiewicz-Kuczera, J.; Yin, D.; Karplus, M. *J. Phys. Chem. B* **1998**, *102*, 3586.

(28) Feller, S. E.; Yin, D.; Pastor, R. W.; MacKerell, J. A. D. *Biophys. J.* **1997**, *73*, 2269.

(29) Wierzbicki, A.; Cheung, H. S. *THEOCHEM* **1998**, *454*, 287.

(30) Mandel, N. S. *Acta Crystallogr., Sect. B: Struct. Sci.* **1973**, *B31*, 1730.

(31) *Cerius<sup>2</sup> Molecular Modeling Software for Materials Research*, Version 4.2; Accelrys, Inc.: San Diego, CA, 2000.

(32) Rappe, A. K.; Goddard, W. A., III. *J. Phys. Chem.* **1991**, *95*, 3358.

(33) Stouch, T. R. *Mol. Simul.* **1993**, *10*, 317.

(34) Essmann, U.; Berkowitz, M. L. *Biophys. J.* **1999**, *76*, 2081.

(35) Petrache, H. I.; Tu, K.; Nagle, J. F. *Biophys. J.* **1999**, *76*, 2470.

(36) Hyvonen, M. T.; Rantala, T. T.; Ala-Korpela, M. *Biophys. J.* **1998**, *73*, 2907.

(37) Bassolino-Klimas, D.; Alper, H. E.; Stouch, T. R. *Biochemistry* **1993**, *12*, 12624.

(38) Shen, L.; Bassolino, D.; Stouch, T. R. *Biophys. J.* **1997**, *73*, 3.

(39) Tieleman, D. P.; Sansom, M. S. P.; Berendsen, H. J. C. *Biophys. J.* **1999**, *76*, 40.

(40) Tieleman, D. P.; Berendsen, H. J. C.; Sansom, M. S. P. *Biophys. J.* **1999**, *76*, 1757.

(41) Tieleman, D. P.; Berendsen, H. J. C.; Sansom, M. S. P. *Biophys. J.* **1999**, *76*, 3186.

(42) Marrink, S.-J.; Berger, O.; Tieleman, P.; Jahnig, F. *Biophys. J.* **1998**, *74*, 931.

(43) Gelb, M. H.; Jain, M. K.; Hanel, A. M.; Berg, O. G. *Annu. Rev. Biochem.* **1995**, *64*, 653.

(44) Hristova, K.; Dempsey, C. E.; White, S. H. *Biophys. J.* **2001**, *80*, 801.

(45) Bigelow, M. W.; Wiessner, J. H.; Kleinman, J. G.; Mandel, N. S. *Calcif. Tissue Int.* **1997**, *60*, 375.